Space Weathering on Inner Planetary Surface Analogues Induced by Swift Multicharged Heavy Ion Bombardment

R. Martinez, A. Agnihotri, E.F. da Silveira, M.E. Palumbo, G. Strazzulla, P. Boduch, Alicja Domaracka, H. Rothard

Space Weathering on Inner Planetary Surface Analogues Induced by Swift Multicharged Heavy Ion Bombardment

R. Martinez[1,2,3], A. Agnihotri[1], E.F. da Silveira[3], M.E. Palumbo[4], G. Strazzulla[4], P. Boduch[1], A. Domaracka[1], H. Rothard[1]

[1] *Centre de Recherche sur les Ions, les Matériaux et la Photonique*

Normandie Univ, ENSICAEN, UNICAEN, CEA, CNRS, CIMAP, 14000 Caen, France

[2] *Physics Department, Universidade Federal do Amapá, Brazil*

[3] *Physics Department, Pontifícia Universidade Católica do Rio de Janeiro,*

Rua Marquês de São Vicente 225, 22453-900, Rio de Janeiro, RJ, Brazil.

[4] *INAF-Osservatorio Astrofisico di Catania, Italy*

ABSTRACT

Silicates are ubiquitous in space. They dominate the surfaces of the inner rocky planets (Mercury in the case of the Solar System), the Moon, and asteroids, forming the major part of the non-volatile material. The physical and chemical properties of the rocky surfaces are determined not only by their initial composition but also by the processes occurring on them. Here we discuss one of these processes; irradiation by energetic cosmic particles that induces many effects among which structural changes and sputtering, the latter contributing to the formation of exospheres. In the current work we report the results of experiments conducted on anorthite, jadeite and nepheline silicates that have been irradiated with energetic heavy ions with the aim to better understand the interaction of galactic cosmic rays, solar wind, and solar energetic particles with planetary and small body surfaces. The sputtering effects induced by energetic (MeV/u) multicharged heavy ions (e.g., ^{105}Rh and ^{140}Ba) were analyzed by the PDMS-TOF-SIMS technique (plasma desorption mass spectrometry - time-of-flight secondary ion mass spectrometry). Positive and negative secondary ionic species are identified: Na^+, K^+, Al^+, Ca^+, SiO_2^-. Ejection of $(SiO_2)_n^-$ and $(AlSi)O_m^-$ cluster series are also observed. Less frequent, negative ion yields are one order of magnitude less than positive ones, or greater, which is the case for nepheline, with 0.671 ions impact^{-1} for positive and 0.126 ions impact^{-1} for negative ions. The results concerning ejection of ionic species show, for instance, that the Na^+/K^+ ratio is ~2.5, which is in very good agreement with that observed in the Hermean exosphere found to be ~2.3.

Keywords: Moon, surface, Mercury, surface; Cosmic rays; Solar wind; Impact processes; Atmospheres, evolution

Silicate Irradiation, Energetic Heavy Ions, Space Weathering, Sputtering, Planetary surfaces.

1. INTRODUCTION

Among materials present in space, silicates are one of the most abundant. In the Solar System (SS), they are present in asteroids, meteorites and comets, where they comprise the major part of the non-volatile material (e.g. Hapke 2001, Strazzulla *et al.* 2005, Nuth & Johnson 2006). Their occurrence in other objects has been reported: in planets and their moons (e.g. Hapke 2001, Gudipati 2014, Cruikshank *et al.* 2015, Helled *et al.* 2020) and in trans Neptunian objects (Brucato *et al.* 2003). For instance, silicates are the dominant component of planet's crust (Henning 2010). In Mercury's crust silicates are even more abundant than iron. The large diversity in composition and structural properties of silicates determines not only the composition and nature of the objects in the SS but also properties and processes occurring on them, like albedo or exosphere's formation. Briefly, silicates play an important role in the cosmic life cycle of matter (Henning 2010).

Similarly to other materials in space, silicates are modified by Solar Wind (SW), Solar Energetic Particles (SEP), and Galactic Cosmic Rays (GCR) irradiation (Strazzulla *et al.* 1995, Davoisne *et al.* 2008). Hereinafter we use the terms cosmic rays (CR) to indicate energetic ions in space. Cosmic ray impacts induce physico-chemical modifications, particularly structural changes (like amorphisation) (Brucato *et al.* 2004, Szenes *et al.* 2010), and sputtering (Wiens *et al.* 1997, Baragiola 2004, Martinez *et al.* 2017). Sputtering is an erosion process that happens to any airless object exposed to the harsh environment of outer space (Brunetto 2009, Pieters & Noble 2016, Longobardo *et al.* 2020). It is of great importance because it causes major changes in optical properties of surfaces, like the Moon, where Space Weathering (SpWe) lowers the albedo, reddens the spectral slope, obscures absorption bands, and generates the characteristic magnetic electron spin resonance features of the lunar regolith (Cassidy & Hapke 1975, Hapke 2001).

SpWe effects due to sputtering have already been studied, in particular the erosion and surface alteration caused by the removal of atoms and/or molecules from a solid surface due to the interaction of projectile ions with target electrons and nuclei, as well as secondary cascades of collisions between target atoms (Sigmund 1981, Plainaki *et al.* 2009). In the Solar System, in several planetary environments, sputtering is one of the most important agents for the surface erosion; it occurs e.g. on Mercury (Cheng *et al.* 1987, Milillo *et al.* 2005, Martinez *et al.* 2017), the Moon (Hunten & Sprague 1997, Wurz *et al.* 2007), Europa (Eviatar *et al.* 1985) and Io (Wiens *et al.* 1997). Sputtering of the mineral components present at the surfaces of Mercury and the Moon appears to be among the most efficient source of sodium and potassium in their exospheres (e.g. Leblanc *et al.* 2007, Killen *et al.* 2008). Na^+ and K^+ ions have been observed in Mercury's exosphere by Earth based and space observations e.g. by the MESSENGER spacecraft (Zurbuchen *et al.* 2008, Paral *et al.* 2010).

Effects induced by energetic ions have been studied in laboratories since several decades with the aim to simulate and cosmic rays induced modifications. In particular to determine the importance of sputtering by solar wind ions on the formation of a sodium exosphere around Mercury and the Moon, Dukes *et al.* (2011) irradiated Na bearing tectosilicates with 4 keV He ions. Specifically space weathering has been analyzed and studied in laboratory; for instance, Marchi *et al.* (2005) performed ion irradiation experiments of silicates and compared laboratory spectra with those of asteroids and meteorites. They found similar mineralogy between most asteroids and meteorites, but different distributions of spectral slopes. All these experiments produced reddening and darkening of reflectance spectra, thus the variation observed in astronomical spectra were interpreted as space weathering induced by solar wind ion irradiation. Fu *et al.* (2012) performed ion irradiation of silicates samples with 50 keV He^+, reflectance spectra at the VIS–NIR range showed also reddening and darkening of samples (for a review see Brunetto *et al.* 2015).

Several silicates were irradiated and analyzed as possible candidates for the surfaces of small objects and planets in the SS. Dukes *et al*. (2011) irradiated with 4 keV He^+ projectiles albite, labradorite, and anorthoclase samples, as well as adsorbed Na layers deposited on albite and on olivine in order to quantify the Na sputtering at the surface and near surface. Nepheline, an aluminosilicate considered to be a good analogue for Mercury's surface (Shimoda *et al.* 2005, Wooden 2008), has also been irradiated with keV/u–MeV/u ion beams and measured sputtering yields and velocity spectra to better understand the evolution of silicate surfaces and the presence of Na and K vapor in the Hermean exosphere (Martinez *et al.* 2017). As an additional process, to simulate the effects caused by micrometeorite bombardment, pulsed intense infrared lasers were used to irradiate olivine and pyroxene targets (Weber *et al.* 2020).

Ion sputtering is an important and active process in many SS planetary environments where a temporary plasma is generated and can precipitate on their surfaces. In this work we present experimental results concerning anorthite, jadeite and nepheline silicates irradiation with energetic heavy ions to contribute to a better understanding of the interaction of energetic cosmic particle irradiation of planetary and small body surfaces. The heavy ion projectiles are fission fragments (FF) emitted by a ^{252}Cf source. Experiments with FF (e.g., ^{105}Rh and ^{140}Ba) with atomic numbers close to that of heavy constituents of CR are indeed a good simulation of effects induced by the heavy ion fraction (a few percent) of cosmic rays (Farenzena *et al.* 2005, Martinez *et al.* 2014). Under these conditions, the FF-silicate interaction yields an electronic (inelastic) stopping power of about 5 keV/nm, i.e. much higher than the nuclear (elastic) stopping power one. The aim of the present work is to provide new insights about compositions of surfaces and exospheres of Mercury, Mars and the Moon, as well as desorption yields of ionic species (sputtering) due to the space weathering caused by cosmic rays. In addition, the results here presented may help to understand future observations of missions like Artemis to the Moon, BepiColombo to Mercury and Perseverance to Mars.

2. SPUTTERING - EXPERIMENTAL METHODS

The experiments were performed at the Van de Graaff Laboratory of the Pontifical Catholic University of Rio de Janeiro (PUC-Rio). The silicate samples were irradiated and analyzed *in situ* by using the technique PDMS-TOF-SIMS (plasma desorption mass spectrometry - time-of-flight secondary ion mass spectrometry). This technique uses as projectiles energetic (~0.5 MeV/u) multicharged heavy ions (e.g., ^{105}Rh and ^{140}Ba) emitted by a ^{252}Cf source. The outline of the set-up is shown in **Fig. 1**. Briefly, it consists of a time-of-flight mass spectrometer with the sample holder located in front of a ^{252}Cf source. The FF impact analysis occurs by transmission mode (the FF passes through the sample). The experiments are performed under high vacuum (pressure ~ 1×10^{-6} mbar). Details of the technique can be found elsewhere (Ponciano *et al.* 2002, 2007). The projectile ions penetrate the target layers deposited on a substrate, a thin carbon foil. The sputtered ions are forward ejected with respect to the incident beam (forward sputtering process) and are extracted by means of an electrostatic field and directed onto a micro-channel plate detector. The induced electron avalanche at the position of the secondary ion impact generates a fast "STOP" signal. In addition, secondary electrons produced at the target backside are accelerated and used to trigger "START" signals. Both the start and the stop signals are feed into a start-stop time-to-digital converter (TDC) to generate TOF mass spectra of the secondary ions.

Nepheline, jadeite and anorthite targets were prepared *ex situ* at PUC-Rio. The different rocks were ground with a mortar and pestle and the grains were glued on carbon foils. With this technique, almost uniform thin films can be produced. The target thicknesses were typically ~ 1 μm determined by means of an optical microscope. In order to reduce surface contamination, the targets were heated *ex-situ*, (T = 60°C for 60 min) to allow evaporation of water and other volatile contaminants and then reintroduced via a rapid airlock into the chamber. Finally the samples were irradiated at room temperature.

2.1 Heavy-ion impact irradiation

Cosmic rays are composed mainly of light ions (protons and α particles), but also of heavier ones (e.g. Fe and Xe). The main physicochemical phenomena that occur when an energetic (keV to GeV) ion impinges a solid are: compaction-amorphisation, electronic excitations (including ionization) in the bulk, chemical reactions, secondary electron emission and sputtering (secondary particle emission). Laboratory investigations about particle–solid interactions are numerous and have used charged energetic particles as projectiles (Brown *et al.* 1984; Baragiola *et al.* 2003; Strazzulla 2011; Raut & Baragiola 2013).

Experimental data from materials irradiated with MeV/u heavy ions is somehow scarce because of the technical difficulties in obtaining these ion beams. In this sense and for certain applications and studies (e.g. ion desorption yield measurements and mass spectrometry) the $^{252}_{98}Cf$ FF nuclei constitute an easily accessible ion source. This particular radioactive nuclide is the most practical source due to its 2.64-yr half-life and affordable price (Macfarlane & Torgerson 1976).

The ^{252}Cf FF mass distribution has a characteristic camel-like shape with maxima at about 105 and 140 u (Nervik 1960; Kiesewetter *et al.* 1992; Schmidt *et al.* 2008). Thus, typically ^{105}Rh and ^{140}Ba, have energies of ~ 0.5 MeV/u and interact with the target atoms depositing energy mainly in the electronic regime. Because the Cf source is sealed for radiological safety reasons, the FF's kinetic energy is reduced by ~ 25% as they pass through the nickel capsule sealing. For the analysis and simulations here presented, the average kinetic energy per nucleon (*E/m*) of ~ 0.5 MeV/u was considered for the FF group. The electronic stopping powers for the three silicates irradiated with H, He, Fe and FF have been calculated with the SRIM code[1] (see **Fig. 2**). Simulations show that Fe and FF projectile distributions are quite equivalent with a maximum stopping power (Bragg peak) at around 1x10^3 eV (10^{-15} atoms^{-1} cm^2) or 7.6x10^2

[1] SRIM code version SRIM-2013.00 (http://www.srim.org).

eV/Å. It is also important to note the stopping powers for H and He projectiles, at this energy, are around two orders of magnitude lower than for Fe or FF ones. **For heavy projectiles like Fe and FF, a small discontinuity feature is observed at 2.5 keV/nucleon, which is due to the SRIM calculation itself. This region is the limit of the TRIM calculation. For lower energies it is simply a straight line (in log-log) extrapolated to zero**.

3. SECONDARY ION FORMATION ON SURFACES

Three silicate targets of astrophysical interest were prepared and irradiated with swift heavy multicharged ions. Anorthite is a mineral silicate species of the tectosilicates subgroup, with formula $CaAl_2Si_2O_8$. It is the calcium end member of the plagioclase feldspar mineral series and may contain traces of Ti, Fe, Na and K. Anorthite, on Earth, can be found in igneous rocks and is abundant on the Moon (Wenk *et al.* 1980, Smyth 1986, Wu *et al.* 2020). Also, feldspars, like anorthite, are the most plausible source of alkali metals in the exosphere of Mercury and may contribute to the calcium signal (Sprague *et al.* 2007, Wurs *et al.* 2010, Domingue *et al.* 2014).

Jadeite is a mineral species from the silicate family, a class of inosilicates, group of pyroxenes whose ideal chemical composition is $NaAlSi_2O_6$. It has a typical Mohs hardness 6.5 to 7.0, depending on the composition, with a specific gravity of about 3. This unusual high density was assumed be due to its occurrence in high-pressure sites; in fact jadeite is formed under high pressure (Harlow *et al.* 2015). In the early Solar System, such high–pressure polymorphs were formed by collisions and impact events on Mars and Moon surfaces (Ohtani *et al.* 2017), and on asteroids like Bennu[2] or the Chelyabinsk meteor, which microscopic

[2] www.nasa.gov/feature/goddard/2002/osiris-rex-unlocks-more-secrets-from-asteroid-bennu

examinations revealed rapid crystallization, meaning that the meteorite is the product of a collision of the original body (Ozawa *et al.* 2014).

Nepheline is a mineral species of the tectosilicate family, a group of feldspathoids: a silica-undersaturated aluminosilicate, containing sodium and potassium with the chemical formula $(Na,K)AlSiO_4$. Nepheline is well suited for simulating the surface of several objects in our Solar System. For instance, it is thought to be formed in meteorites parent bodies, by late thermal alteration event(s) of chondrules, as in the Allende CV3 meteorite (Lumpkin 1980, Shimoda *et al.* 2005, Ichimura *et al.* 2017). Also, among other silicate minerals discovered in Stardust Mission return samples, from comet 81P/Wild, nepheline was observed (Wooden *et al.* 2008). In planetary surfaces, nepheline also may be present. According to Emery *et al.* (1998), spectra analysis from Mercury's surface indicates possible alkali-rich volcanic, like nepheline. They also show features common to igneous nepheline-bearing alkali syenite (Sprague 1998).

3.1. Sputtering of Positive Ions.

Positive ion mass spectra from the silicate samples irradiated with energetic heavy ions (FF) are shown in **Fig. 3**. They are characterized by the presence of the three hydrogen peaks, H^+ H_2^+ and H_3^+, being an unavoidable contaminant in every vacuum chamber. Another characteristic peak in all positive spectra is at 23 u, which is assigned to the Na^+ ion.

In particular, nepheline spectrum is characterized by mass peaks at 39 u and 63 u which can be assigned to K^+ and $(Na_2O)H^+$. A small peak is observed for Al^+ at 27 u. Also a cluster series of molecules due to atom recombination upon ejection can be observed at 81 u, 97 u, 113 u, 129 u and 145 u mass peaks assigned to $Al_3O_n^+$ series, with n = 0 to 4. For the peak at mass 103 u, the $AlSiO_3^+$ species is a plausible candidate.

On the other hand, anorthite and jadeite positive mass spectra are less rich in species. Besides the characteristic peaks, some others can be observed like the Al^+, K^+ and Ca^+ for

anorthite, and Al^+, K^+, $NaAl^+$ and $(Na_2O)H^+$ for jadeite. For silicates containing Na in its structure, the species $(Na_2O)H^+$, at 63 u, seems to be ubiquitous.

3.2. Sputtering of Negative Ions

Negative ion mass spectra are more abundant in species than positive ones. **Fig. 4** shows the mass spectra, from 50 to 185 m/z, for the three silicates. Interesting sputtered species can be observed in the three spectra, like the silicon dioxide (SiO_2) forming a cluster series, the $(SiO_2)_n^-$ with n = 1 to 3, being important for all the three silicates. Another example of sputtered species is the aluminum silicon molecule linked to oxygen atoms, forming the cluster series $(AlSi)O_m^-$, with m = 0 to 8, being more important for nepheline. The $Al(SiO_2)_2O_2^-$ molecule is also observed in the three spectra at 179 u.

In addition, each spectrum shows specific species for each silicate. For instance, the $(SiO_2)_2O^-$ molecule is observed when anorthite and jadeite targets are irradiated, while the anorthite spectrum shows the CaO_2^- specific species.

3.3. Sputtering Yields

Regarding the mechanism of ion induced desorption from planetary surfaces, the total desorption yield (Y_{tot}), which is defined as the number of molecules, neutral or ionized, ejected per impact, results from a sequence of events after the ion-surface interaction. Energetic heavy ions with velocities higher than the Bohr velocity (25 keV/u) transfer most of their energy to the target electrons. In insulators, the electronic excitations can lead to repulsive states, which cause, at the target surface, particle ejection. The PDMS-TOF-SIMS technique is suited for the fragmentation pattern study during prompt induced desorption (i.e. sputtering), which occurs on time-scales of $\sim 10^{-11}$ s after the ion impact.

Table 1 shows the absolute desorption yields (number of desorbed ions per impact) for the most relevant positive and negative ion species. In addition, **Fig. 5** shows bar spectra of

absolute desorption yields for positive ions, for each silicate, with mass-to-charge ratio up to 70 m/q. Since the majority of desorbed species have q = 1, the ratios m/q are in practice substituted by the ion masses, generating mass spectra. To estimate the absolute desorption yields for each discrete m/q, a flux of 60 ± 2 FF impacts s^{-1} in the solid angle of the sample was used. Thus an analysis of a number of fragments of the cationic and anionic species, produced by ionization, dissociation and recombination processes, was performed.

The number of electronic excitations is proportional to $S_e = (dE/dx)_e$ (electronic stopping power). When the excitation density is high, cooperation between close excitation events along the nuclear track enhances the sputtering yields. Based on experiments, a power law ($Y \propto S_e^n$) dependence of the sputtering yield (Y) on the energy deposition per unit path length (S_e) has been found. The range of reported powers (n) is wide, from 1 to 6, and they may be different for ejected ions and neutrals. For instance Brown *et al.* (1984) and Shi *et al.* (1995) have shown the quadratic dependence of the total (ionic and mainly neutral) sputtering yield (Y_{tot}) on the energy deposition per unit path length (S_e), with MeV light ions (mainly using water ice-targets). Seperuelo-Duarte *et al.* (2010) extended the sputtering yield measurements on CO ice to heavy ion beams (50 and 537 MeV Ni), confirming the power law $Y_{tot} = a\, S_e^2$ for four order of magnitudes on S_e and six on Y. Regarding only ion yield dependence, de Barros *et al.* (2011), through H_2O ice irradiations, found a third power dependence of ion-sputtering yields on S_e. Concerning other materials, Toulemonde *et al.* (2020) have shown a quartic dependence of the total sputtering yield (Y_{tot}) of lithium fluoride with swift heavy ions as projectiles, and Hijazi *et al.* (2014) a quadratic dependence for secondary ions (low Z projectiles), i.e. $Y_{ion} \propto S_e^2$.

Fig. 6 (upper panel) shows an estimate of the ion-sputtering yields for anorthite, jadeite and nepheline; considering the *quadratic power dependence*. The inset plot shows also the experimental values. The ion beam used for these simulations is the ^{140}Ba (0.46 MeV/u), which is considered as representative of the heavy FF mass group. Vertical arrows indicate the average

energy per nucleon. Thus, **Fig. 6** shows the corresponding total ion sputtering yield occurring at E/m = 0.46 MeV/u, for ^{140}Ba, assuming the quadratic power law to be fixed in this energy regime, related to the physical process of the electronic sputtering. The factor a in $Y_{ion} = a\ S_e^2$ **is determined by using the experimental data and used to fine-tune the SRIM data of Fig. 2, to all energies**. It varies for each target, but for silicate materials is approximately the same, being on the order of 5.0×10^{-9} (Å/eV)^2. The lower panel of **Fig. 6** shows three simulations of the nepheline ion sputtering yield (Y_{ion}) dependence on the energy deposition per unit path length (S_e) following the power law model ($Y_{ion} \propto S_e^n$). In fact, ion irradiation experiments with one silicate at several ion energies are being carried out. This will let us determine the right dependence of Y_{ion} on S_e, for silicates.

It should be noted that the same trend observed in **Fig. 2** is observed here as well, which means that heavy ions in the MeV/u range around the Bragg peak are several orders of magnitude more efficient for inducing desorption than protons and α particles, at the same velocity (E/m). This indicates that the very high desorption yields of MeV/u heavy ions must be taken into account for silicates chemical processing and space weathering.

4. ASTROPHYSICAL IMPLICATIONS

Space weathering of surfaces due to irradiation effects plays an important role in the composition/modification of exospheres, mainly in objects where its magnetic field is weak or does not exist. Mercury and the Moon possess very thin atmospheres (exospheres) and magnetospheres weak enough to allow energetic charged particles to impinge directly into their surfaces depositing energy and physically altering materials present on them (Wurz *et al.* 2010, Paral *et al.* 2010, Milillo *et al.* 2010, Domingue *et al.* 2014). Thus space-weathering processes are tied to the exposure of a planetary surface to its space environment, generating and maintaining a surface-bounded exosphere. In this scenario, desorption of neutral and ionic

species plays an important role. The current results concern the ionic contribution.

4.1. Sputtering in Planetary Surfaces

Desorbed species due to sputtering contribute to the exospheres, reflecting - in some extent - the surface composition. Particularly, the presence of low energy ions in the exospheres near the surface of airless planetary bodies such as the Moon, Mercury, and asteroids should be largely indicative of the planetary surface elemental composition (Johnson and Baragiola 1991, Dukes and Baragiola 2015, Martinez 2017).

a) Effects on the Moon

The Moon has a reasonable gravity and no magnetic field; its surface is subjected to solar wind, solar energetic particles, and galactic cosmic ray irradiation, with a much higher flux than asteroids in the main belt. The lunar exosphere is a region of space above the surface reaching an altitude of ~100 km, with an atomic density as low as 10^6 cm^{-3} (Dukes and Baragiola 2015). Via mass spectrometer measurements of the AMPTE, WIND and SELENE missions, charged species have been observed in lunar exosphere. They have locally identified ions such as Ar^+, Na^+, K^+, Si^+, Al^+, C^+, and O^+ (Hilchenbach *et al.* 1993, Stern 1999, Yokota *et al.* 2009, 2014). More recently, measurements by the LADEE mission identified significant detections of lunar ions with mass per charge of 2, 4, 12, 20, 28, 39, and 40, moderate detections with 14 and 23, and weak detections with 24, 25, and 36 (Halekas *et al.* 2015). For these experiments, they used an outward pointing viewing geometry, ensuring that these ions originate from the exosphere.

Thus, determining lunar sputtering yields of ionic species is well justified. According to Dukes *et al.* (2015), sputtered ions may be more important in lunar exosphere in the sense that they continue to interact with the lunar surface by charging or neutralizing regions of the regolith and by self-sputtering (Poppe *et al.* 2013). Additionally, cation and anion yields are

richer as they show molecular series. The Moon's exosphere may depend on this too, in particular silicon oxides series, as shown later.

Considering that composition and stoichiometry of the targets are known and that, in first approximation, the sputtered species are proportional to the initial stoichiometry (Dukes *et al.* 2011), the sputtering yield of a specific species would represent a percentage of the initial (total) concentration, indicating the loss (depletion) of a particular element of the sample (Williams 1984, Dukes *et al.* 2011). In addition, the ion fraction of the sputtered species must be taken into account in this analysis. Neutrals are expected to be more abundant than ions. While sputtering measurements and model predictions for oxides and minerals have shown ionic fraction values close to 1, for several species (Benninghoven *et al.* 1972, Andersen *et al.* 1972). Similar SIMS measurement results were obtained by Elphic *et al.* (1991) by irradiating lunar soil analogs. Steinbrüchel *et al.* (1980, 1981) measured ion fractions of 0.4–0.8 from metal oxides, and more recently Dukes *et al.* (2011) have obtained results well in between by irradiating tectosilicates. A fraction of 0.5 will be considered here.

The PDMS-TOF-SIMS analyses of lunar soil analogs show an important surface depletion of Na^+. For Jadeite (with 10% of Na by number), it is observed ~3.6% surface depletion (Y_{ion} = 0.363 Na ions impact^{-1}). And if we consider the, sputtered but not detected, Na^0 species, the Na depletion increases to ~7.2%. For Nepheline (15% Na by number), a ~3.1% depletion is observed (0.251 ions impact^{-1}); and considering the neutral fraction, an erosion of ~6.2% is found; 14% less than for Jadeite. Na is not supposed to exist in Anorthite, but this mineral shows a very small emission yield of Na^+ (0.0417 ions impact^{-1}) because it is a common impurity. Aluminum depletion is expected to be quite the same for the three silicates samples; Anorthite (with 15% of Al by number) shows a relative important surface depletion of ~0.51% (0.0340 ions impact^{-1}), ~1.02% taking into account neutrals. And Jadeite (10% Al by number) Al^+ is depleted by ~0.14% (0.0138 ions impact^{-1}), 0.28% with neutrals; ~70% less depletion

than the former. But interestingly, Nepheline (12.5% Al by number) shows very low Al^+ emission, of the order of 0.0037 ions impact^{-1}, implying a depletion of 0.05% (0.1% including neutrals); ~10 times lower than the one for Anorthite, for instance. This may indicate that planetary surfaces containing this kind of aluminosilicate will maintain exospheres with low quantities of Al. Concerning potassium, the ion depletion occurs for Nepheline (12% of K by number) sample only, with a relative high ~1.28% (0.1023 ions impact^{-1}) or ~2.56% considering neutrals. Anorthite and Jadeite samples show low emission yield of potassium ion since it is a common impurity. Similarly, Ca^+ ion is only observed for Anorthite (7.7% of Ca by number) targets as expected, with a moderate ion depletion of ~0.25%, or ~0.5% with neutrals (0.0302 ions impact^{-1}).

b) Effects on the Mercury planet

Mercury has a relative strong gravity field. The gravitational acceleration at the surface is approximately 3.697 m s^{-2}, more than twice the value on the Moon (Wurz 2010, Paral 2010). Its magnetic field intensity is about 1% of the Earth's field intensity at the surface (Takahashi 2019). Thus, Mercury also presents an interesting environment to study and understand the interactions between the SW, SEP, and GCR, planetary surfaces and surface-bounded atmosphere as mediated by a not so strong internal magnetic field (Milillo *et al.* 2005). Although there is no direct information available about how space weathering affects Mercury's regolith, like returned samples (Domingue *et al.* 2014), Zurbuchen *et al.* (2008) suggest clues on the composition of Mercury's ionized exosphere: the Fast Imaging Plasma Spectrometer (FIPS), the low energy portion of the Energetic Particle and Plasma Spectrometer (EPPS), detected Na^+, O^+, and K^+ species, among other possible ions and molecular ions, consistent with expectations from observations of neutral species (Zurbuchen *et al.* 2008, Paral *et al.* 2010).

The PDMS-TOF-SIMS analyses of analogs for the Hermean soil shows relatively high sputtering yields of Na^+ and K^+ species, depending on the analog. As stated by Dukes *et al.*

(2015) and others, sodium and potassium are the predominant species sputtered from the Mercury surface (Potter *et al.* 1986, 1987, 1997, Gamborino 2019). For the first analog, Anorthite, those two species are natural contaminants. However, it could be a good source of ionized calcium Ca^+, since it has already been detected in the Hermean exosphere by the MESSENGER mission, with abundances comparable to that of K^+ (Zurbuchen *et al.* 2008). The Ca^+ sputtering yield here measured is of the order of 0.0302 ions impact^{-1}, which is lower than necessary to explain the observation by Zurbuchen *et al.* (2008). In fact, Ca should be released less efficiently than Na and K due to its bonds with oxygen atoms in the bulk/surface. On the other hand, the Jadeite sample shows an interesting Na^+/Al^+ ratio of ~26.3. The Na/Al ratio (neutral atom ratio) was found to be between 1.3 and 1.7 (Wurz *et al.* 2010, Domingue *et al.* 2014). Comparing to the ionic ratio, those values are in agreement if we consider that Na is more likely to be ionized: the Al ionization energy (5.99 eV) is higher than that of Na (5.14 eV). On the contrary, Zurbuchen *et al.* (2008) did not report any observation of Al^+.

Concerning the sodium and potassium emission, the spatial distribution of the Na/K exospheric column density ratio is temporally variable due to several factors like the interactions of solar wind and magnetosphere. In this sense, ratios already observed or calculated vary in a wide range with values ranging from ~26 to ~300 (Doressoundiram *et al.* 2010, Leblanc *et al.* 2011, Domingue *et al.* 2014). Observations of Na^+/K^+ ratio reported by Zurbuchen *et al.* (2008) found a value of ~2.3, which is in very good agreement with the ~2.5 value that we measured for nepheline (see **Table 1**). This value is also in agreement with calculations made to estimate densities of species in the exosphere of Mercury; Wurz *et al.* (2010) found ionization Na^+/K^+ ratio of 2.4. This phenomenon may be due to the Na higher ionization energy.

4.2. Negative Ions in Exospheres

The formation processes of negative ions at surfaces relevant to astrophysical environments are not well studied yet. Moreover, collisional electron attachment processes would not be considered important, as pressures in most environments are far too low for this process to be significant (Millar *et al.* 2017). However, particle-stimulated emission of anions from surfaces has been observed and studied in laboratory, at low temperatures and ultra high vacuum (e.g. de Castro *et al.* 1997, Andrade *et al.* 2008, Martinez *et al.* 2012, 2014, Oliveira *et al.* 2021).

Different mechanisms for the formation of negative ions have been proposed. Probably the most important is the electron attachment, initiated by free electrons (Millar *et al.* 2017). Indeed, when heavy multicharged ions (e.g. cosmic rays, FFs) interact with a solid, emission of secondary electrons occur together with neutral and ionic species (Iza *et al.* 2005, Martinez *et al.* 2006); a plasma is temporary formed, favoring electron attachment (Macfarlane & Torgerson 1976, Oliveira *et al.* 2021). In other words, electron attachment cross sections are enhanced on the surface in part because of multiple scattering of electrons and adjacent species.

Laboratory results have demonstrated, for different materials, that cationic species desorption yields are much higher than anionic ones, at around two or three orders of magnitude greater (Farenzena *et al.* 2006, Martinez *et al.* 2014). On the other hand, the here obtained absolute desorption yields Y_i (positive and negative ions, and the sum of all of them; see **Table 2**), show that, when silicate targets are irradiated by energetic heavy multicharged ions (cosmic rays analogs), high emission rates of SiO_2^- and O^- are observed, turning almost comparable the sputtering yields of cations and anions. Silicates are built of the same basic structural units, the SiO_4 tetrahedra. Metal cations in the silicate network leads to a partial destruction of the O bridges and the formation of nonbridging O (Henning 2010). This fact and the electron affinity of silicon dioxide (0.9 eV) favor the outstanding emission of SiO_2 and O anions (Williams 1965, Ballarotto *et al.* 2002). Accordingly, the three samples analyzed in this work confirm the high

emission yields of SiO_2 and O mainly observed as aggregates or ion cluster series $(SiO_2)_n^-$ and $(AlSi)O_m^-$, as presented before. Molecular cluster emission from surfaces via sputtering, with astrophysical implications, has already been discussed before (Killen *et al.* 2005, 2007, Martinez *et al.* 2017). Recently, molecular aggregates of water (cosmic water nanoclusters) have been considered to explain several processes occurring in the Universe (Johnson 2021).

Mainly after the collected samples during the Apollo missions, Moon surface composition became very well known (Ringwood 1976, Dukes *et al.* 2015). Analyzes of those samples have also revealed that silicon dioxide is one major component, others being $A1_2O_3$, CaO and Na_2O. Moreover, Gu *et al.* (2018) reported the analysis of Apollo 15 soil grains by transmission electron microscopy, displaying silicon dioxides *nanoparticles*. Nevertheless, they state that those nanoparticles were not formed due to solar-wind generated vapor deposit or irradiated rim. In the current work, high emission yield of SiO_2 molecular clusters is observed when silicates are irradiated by heavy ions, which may indicate a molecular cluster redeposition. As mentioned before, the Moon's exosphere was analyzed by the LADEE spacecraft (ARTEMIS mission) and several lunar cations were identified (Halekas *et al.* 2015), proving an ionic exosphere. Nevertheless no anion was reported.

On the contrary, no returned samples or other direct information is available about Mercury's regolith and how it was affected by space weathering. In fact, Mariner 10 and MESSENGER missions and ground-based observations have given us information about surface and exosphere compositions. Ground-based observations of Mercury's surface indicate a heterogeneous surface composition with SiO_2 content ranging from 39 to 57 wt%. Also it is thought to be covered with highly space-weathered silicate material (Sprague *et al.* 2007). Fly-bys of the MESSENGER spacecraft provided insight into the spatial distribution of the heavy ion exosphere around the planet (Paral *et al.* 2010). More specifically, the Si^+ abundance observed is too high, which means its source is either Mercury's surface or its exosphere

(Zurbuchen *et al.* 2008). Likewise, no negative ions were reported until now. In other respect, sputtering of atomic or molecular clusters have not been observed directly in Mercury's exosphere, but it has been proposed that a significant contribution to the Ca exosphere arises from sputtered CaO molecules (aggregates) (Killen *et al.* 2005). This is in agreement with the present results concerning Anorthite sample, from which CaO_2^- ions were emitted ($CaO + O^- = CaO_2^-$).

4.3. Ionic Sputtering Rate

The sputtering rate of ionic species by cosmic rays $R_{S,CR}$ of planetary surfaces analogues can be determined by adapting the analysis made by Mennella *et al.* (2003) and others (Godard *et al.* 2011, Dartois *et al.* 2017). Thus, to extend and apply the current results to astrophysical environments, like planetary surfaces, the total ionic sputtering yields ($\boldsymbol{Y_{i,total}}$) must be summed over the cosmic ray ion abundances and energy distribution contributions:

$$R_{S,CR} = \sum_{Z} \int_{E_{min}}^{\infty} Y_{i,total}^{CR}(E,Z) \frac{dN}{dE}(E,Z) dE \qquad (1)$$

where the second term of the integral is the differential flux of the cosmic ray element of atomic number Z, with a cutoff in energy E_{min} set at 100 eV/u. The differential cosmic ray flux is given by the functional form given by the spectral shape data obtained from four instruments on NASA's Advanced Composition Explorer (ACE) (Mewaldt *et al.* 2001, 2007). Their data are empirically fitted by:

$$\frac{dN}{dE}(E,Z) = A_1 e^{-\eta \frac{E}{m}} + \frac{A_2}{\left(\frac{E}{m}\right)^2} \qquad (2)$$

where A_1 and A_2 are normalizing constants **at a distance of 1 au** (= 5.0×10^8 MeV^{-1} cm^{-2} s^{-1} and 2.0×10^{-2} MeV u^2 cm^{-2} s^{-1} respectively), η ~ 2.4 x 10^3 u MeV^{-1}, E/m is the cosmic ray kinetic energy in MeV per nucleon, and m is the ion's mass (de Barros *et al.* 2011). **Fig. 2** displays SRIM code predictions for the expected stopping power (S_e) as a function of the atomic

number Z and of the energy per nucleon E/m, and **Fig. 6** (upper panel) the relation established in Section 3.3, linking the total ionic sputtering yield $Y_{i,total}(E,Z)$ to $S_e(Z,E)$ through the relation $Y_{ion} = a\ S_e^2$. This allows determination of the total sputtering yield of ionic species when silicates are irradiated by cosmic ray particle analogues. By applying Eq. (1), the sputtering rate as a function of the cosmic particle (i.e., galactic CR and Solar particles) energy was determined as showed in **Fig. 7**, which is the product of cosmic particle flux times the total sputtering yield. At 1 au the differential flux of cosmic particles (galactic cosmic rays, solar wind, solar energetic particles) is given by the functional form given by the spectral shape data obtained from the instruments on NASA's Advanced Composition Explorer (ACE) (**Mewaldt *et al.* 2001, 2007**). **The curves plotted in Fig. 7 are the result of the product of the cosmic particle flux times the total sputtering yield. The huge peak at E/m < 5 keV/u, reflects the fact that at these energy values the flux is very high (due to solar wind ions) but the sputtering yield is low. However we have to keep in mind that in the keV regime the nuclear stopping power is higher than the electronic stopping power and the relation $Y_{ion} = aS_e^2$ might no longer be valid. As pointed out by Martinez *et al.* (2019), the dependence of the sputtering yield on the total stopping power and, in particular, the contribution of the nuclear stopping power is not yet well known and further experiments are needed to be fully understood. In Eq. (2) the parameters A_1 and A_2 include the dependence of the flux on Z. The values of A_1 and A_2 adopted in our calculations are taken from Table 9 in de Barros *et al.* (2011) where the A_1 and A_2 values for various ions are reported taking into account their different abundance. In the present work, FF "simulate" Fe projectiles. To see the effects in space, we take into account the Fe abundance in space and correct the yield effects by its dependence on the higher stopping power of FF in relation to Fe**.

Results for the three silicate samples are very similar that seem to merge in one curve, for each projectile (Fe and FF). At cosmic particle energies of 0.46 MeV/u, silicate ionic sputtering rate $R_{s,CR}$ = 6.3 x 10^{-2} particles cm^{-2} s^{-1} is found. The corresponding sputtering timescales (τ =

$1/R_{S,CR}$) associated with the destruction rates for E = 0.46 MeV/u are around $\tau \sim 15.9$ s cm^2 ion^{-1}. Astrophysical implications for the evolution of planetary silicates subjected to cosmic rays, providing information on potential species to be released, show that silicates dust grains are relatively resilient against sputtering by cosmic rays.

The sputtering rate here estimated is valid for the Moon's surface (1 au). The evaluation of the sputtering rate at Mercury's surface (0.39 au) is more complex. In fact the energy spectrum and the flux of galactic cosmic rays is approximately the same everywhere in the Solar System. Also the energy spectrum of solar wind does not change but its flux varies as the inverse of the square of the distance from the Sun being then much larger at Mercury than at the Moon. In addition, Mercury's magnetic field partially inhibits the direct access of solar energetic ions to the surface. Then, sputtering rates and timescales on Mercury will be estimated when reliable data on cosmic particle flux on the surface of Mercury become available.

5. CONCLUSIONS

In order to determine ion-sputtering yields of astrophysical silicates bombarded by solar wind, solar energetic particles, and galactic cosmic rays, laboratory experiments with silicate analogs have been performed. Anorthite, Jadeite and Nepheline were exposed to ^{252}Cf fission fragments and the absolute ion desorption yields have been measured and analyzed by the PDMS-TOF-SIMS technique. Current results show several ionic species emission due to this interaction, which is dependent on the irradiated silicate (see **Table 1**).

Desorbed species, neutral and ionic, contribute to exospheres, also reflecting - in some extent - surface composition. In this sense, the current results may represent sputtering in planetary surfaces. In fact, the observed ion species are the likely constituents of cosmic body exospheres and the ion sputtering yield, Y_{ion}, reflects the magnitude of this depletion, which is sample dependent. Indeed, PDMS-TOF-SIMS results from Anorthite sample, analogue of *the Moon's* crust, exhibit comparable and relative moderate depletions of Al^+ and Ca^+ (~0.51% and ~0.25% respectively). On the other hand, Jadeite and Nepheline reveal low and very low depletion rates of Al^+, respectively (~4 to ~10 times lower than the one for Anorthite). This indicates that planetary surfaces containing this kind of aluminosilicates will maintain exospheres with low quantities of Al^+. Observation of Na^+ in lunar exosphere indicates that others silicates must be present. Jadeite proves important surface depletion of Na^+, with ~3.6% surface depletion (Y_{ion} = 0.363 ions impact^{-1}). Similarly, Nepheline shows a ~3.1% depletion of Na^+ at the surface. The observation of the sodium cation is in agreement with initial measurements of the AMPTE, WIND and SELENE missions and, more recently, with measurements by the LADEE mission.

The PDMS-TOF-SIMS analyses of analogs for the Hermean soil evidence a Na^+/Al^+ ratio of ~26.3. This is unexpected because the Na/Al ratio (neutral atom ratio) was found to be between 1.3 and 1.7 (Wurz *et al.* 2010, Domingue *et al.* 2014). Comparing to the ionic ratio,

those values may be in agreement if we consider that Na is more likely to be ionized. Unexpectedly, Zurbuchen *et al.* (2008) did not report any observation of Al^+. Concerning the sodium and potassium emission, observations of Na^+/K^+ ratio reported by Zurbuchen *et al.* (2008) found a value of ~2.3, which are in very good agreement with the ~2.5 current results measured with Nepheline. This value is also in agreement with calculations made to estimate densities of species in the exosphere of Mercury; Wurz *et al.* (2010) found an ionization Na^+/K^+ ratio of 2.4.

The three analyzed samples confirm the high anion emission yields of SiO_2 and O mainly observed as aggregates or ion cluster series $(SiO_2)_n^-$ and $(AlSi)O_m^-$. This could be explained by the sputtered species electron affinity and by the temporary plasma formation when heavy multicharged ions (e.g. cosmic rays, FFs) interact with a solid surface (emission of secondary electrons together with neutral and ionic species). This enhances electron attachment cross sections on the surface, in part because of multiple scattering of electrons and adjacent species. Gu *et al.* (2018) reported the presence of silicon dioxides *nanoparticles* in Apollo 15 soil grain samples. The emission of $(SiO_2)_n$ aggregates suggests a molecular cluster redeposition in the form of "*nanoparticles*". Nevertheless no anion was observed yet; neither on the lunar nor on the Hermean surfaces.

The total ion yield ($Y_{t,ion}$) was also determined by means of the quadratic power dependence of ion-sputtering yields on S_e, i.e. $Y_{ion} = a\,S_e^2$ (**Fig. 6**). Sputtering rate dependence on the cosmic ray energy is analyzed by combining the total ion yield $Y_{t,ion}(E,Z)$ and the differential cosmic ray flux $dN/dE(E,Z)$ given by the spectral shape data. Results for the three silicates irradiated with Fe and FF projectiles show comparable values and seem to merge in only one curve for each beam. Silicate sputtering rate of 6.3×10^{-2} particles cm^{-2} s^{-1} at cosmic ray energies of 0.46 MeV/u is found. The corresponding sputtering timescales is around $\tau \sim$

15.9 s cm^2 ion^{-1}. These results indicate that the evolution of planetary silicates subjected to cosmic rays, like silicates dust grains, are relatively resilient against sputtering by cosmic rays.

Ion irradiation experiments with one silicate at several ion energies are being carried out. This will let us determine or confirm the dependence of Y_{ion} on S_e, for silicates. In addition other silicates will be irradiated to confirm the anion emission values and its implication for astrophysical environments.

The presented results would be useful in understanding the results expected by the European space mission BepiColombo that will reach Mercury in December 2025. In fact among the scientific instrumentation on board the spacecraft there is SERENA 'Search for Exospheric Refilling and Emitted Natural Abundances'. It will investigate the complex particle environment of the Mercury'-s exosphere including thermal and directional neutral ionized species (see e.g. Orsini *et al.* 2010).

Acknowledgements

The French-Brazilian exchange program (Capes-Cofecub) and the Brazilian agencies FAPERJ (PDS-2020 Program) and CNPq (INEspaço) are acknowledge for partially support. This study was financed in part by the Coordenação de Aperfeiçoamento de Pessoal de Nível Superior - Brasil (CAPES) - Finance Code 001. This research has been partially supported by the Italian Space Agency (ASI) contract n. I/081/09/0.

References:

Andersen, C. A.; Hinthorne, J. R. (1972)
Ion Microprobe Mass Analyzer
Science, 175, 853

Andrade, D. P. P., Boechat-Roberty, H. M., da Silveira, E. F., *et al.* (2008)
Astrophysical Icy Surface Simulation under Energetic Particles and Radiation Field in Formic Acid
The Journal of Physical Chemistry C, 112, 11954

Ballarotto, V. W. (2002)
Photoelectron emission microscopy of ultrathin oxide covered devices
Journal of Vacuum Science & Technology B, 20, 2514

Baragiola, R. A. (2004)
Sputtering: survey of observations and derived principles
Royal Society of London Transactions Series A, 362, 29

Benninghoven, A.; Mueller, A. (1972)
Secondary ion yields near 1 for some chemical compounds
Physics Letters A, 40, 169

Brown, W. L.; Augustyniak, W. M.; Marcantonio, K. J.; Simmons, E. H.; Boring, J. W. *et al.* (1984)
Electronic sputtering of low temperature molecular solids
Nuclear Instruments and Methods in Physics Research Section B, 1, 307

Brucato, J.R.; Strazzulla, G.; Baratta, G.; Mennella, V.; Colangeli, L. (2003)
Laboratory Studies on Silicates Relevant for the Physics of TNOs
Earth, Moon, and Planets, 92, 307

Brucato, J.R.; Strazzulla, G.; Baratta, G.; Colangeli, L. (2004)
Forsterite amorphisation by ion irradiation: Monitoring by infrared spectroscopy
Astronomy and Astrophysics, 413, 395

Brunetto, R. (2009)
Space Weathering of Small Solar System Bodies
Earth Moon Planet, 105, 249

Brunetto, R.; Loeffler, M. J.; Nesvorný, D.; Sasaki, S.; Strazzulla, G.
Asteroid Surface Alteration by Space Weathering Processes
In Asteroids IV, Eds. Michel, P.; *et al.* pp. 597–616. University of Arizona Press, 2015, 597-616

Cassidy, W. and Hapke B. (1975)
Effects of darkening processes on surfaces of airless bodies
Icarus, 25, 371

Cheng, A. F.; Johnson, R. E.; Krimigis, S. M.; Lanzerotti, L. J. (1987)
Magnetosphere, exosphere, and surface of mercury
Icarus, 71, 430

Cruikshank, D. P.; Grundy, W. M.; DeMeo, F. E.; Buie, M. W.; Binzel, R. P. *et al.* (2015)
The surface compositions of Pluto and Charon
Icarus, 246, 82-92

Dartois, E.; Chabot, M.; Pino, T.; Béroff, K.; Godard, M.; Severin, D.; Bender, M. *et al.* (2017)

Swift heavy ion irradiation of interstellar dust analogues. Small carbonaceous species released by cosmic rays
Astronomy & Astrophysics, 599, A130

Davoisne, C.; Leroux, H.; Frère, M.; Gimblot, J.; Gengembre, L.; Djouadi, Z. *et al.* (2008)
Chemical and morphological evolution of a silicate surface under low-energy ion irradiation
Astronomy and Astrophysics, 482, 541

de Barros, A. L. F.; Farenzena, L. S.; Andrade, D. P. P.; da Silveira, E. F.; Wien, K. (2011)
Secondary Ion Emission from Water Ice at 10–130 K Induced by MeV N_2^+ Ions
The Journal of Physical Chemistry C, 115, 12005

de Barros, A.L.F.; Domaracka, A.; Andrade, D.P.P.; Boduch, P.; Rothard, H.; da Silveira, E.F. (2011)
Radiolysis of frozen methanol by heavy cosmic ray and energetic solar particle analogues
Monthly Notices of the Royal Astronomical Society, 418, 1363

de Castro, C. C.; Bitensky, I. S.; da Silveira, E. F. (1997)
Desorption of H^- ions from solid surfaces induced by MeV ion impact
Nuclear Inst. and Methods in Physics Research, B, 132, 561

Domingue, D.L.; Chapman, C.R.; Killen, R.M.; Zurbuchen, T.H.; Gilbert, J.A. *et al.* (2014)
Mercury's Weather-Beaten Surface: Understanding Mercury in the Context of Lunar and Asteroidal Space Weathering Studies
Space Science Reviews, 181, 121

Doressoundiram, A.; Leblanc, F.; Foellmi, C.; Gicquel, A.; Cremonese, G.; Donati, J. -F. *et al.* (2010)
Spatial variations of the sodium/potassium ratio in Mercury's exosphere uncovered by high-resolution spectroscopy
Icarus, 207, 1

Dukes, C. A.; Chang, W.; Famá, M.; Baragiola, R. A. (2011)
Laboratory studies on the sputtering contribution to the sodium atmospheres of Mercury and the Moon
Icarus, 212, 463

Dukes, C. A.; Baragiola, R. A. (2015)
The lunar surface-exosphere connection: Measurement of secondary-ions from Apollo soils
Icarus, 255, 51

Elphic, R. C. ; Funsten, H. O., III ; Barraclough, B. L. ; McComas, D. J. ; Paffett, M. T. *et al.* (1991)
Lunar surface composition and solar wind-Induced secondary ion mass spectrometry
Geophysical Research Letters, 18, 2165

Emery, J. P.; Sprague, A. L.; Witteborn, F. C.; Colwell, J. E.; Kozlowski, R. W. H. *et al.* (1998)
Mercury: Thermal Modeling and Mid-infrared (5-12 μm) Observations
Icarus, 136, 104

Eviatar, A.; Bar-nun, A.; Podolak, M. (1985)
Europan surface phenomena
Icarus, 61, 185-191

Farenzena, L. S.; Iza, P.; Martinez, R.; Fernandez-Lima, F. A.; Duarte, E. Seperuelo; Faraudo, G. S.; Ponciano, C. R.; Homem, M. G. P.; de Brito, A. Naves; Wien, K.; da Silveira, E. F. (2006)
Electronic Sputtering Analysis of Astrophysical Ices
Earth, Moon, and Planets, 97, 3-4, 311

Fu, X.; Zou, Y.; Zheng, Y.; Ouyang, Z. (2012)

Effects of space weathering on diagnostic spectral features: Results from He^+ irradiation experiments
Icarus, 219, 630-640

Gamborino, D.; Vorburger, A.; Wurz, P. (2019)
Mercury's subsolar sodium exosphere: an ab initio calculation to interpret MASCS/UVVS observations from MESSENGER
Annales Geophysicae, 37, 455

Godard, M.; Féraud, G.; Chabot, M.; Carpentier, Y.; Pino, T.; Brunetto, R.; Duprat, J.; *et al.* (2011)
Ion irradiation of carbonaceous interstellar analogues. Effects of cosmic rays on the 3.4 µm interstellar absorption band
Astronomy & Astrophysics, 529, A146

Gu, L.; Zhang, B.; Hu, S.; Noguchi, T.; Hidaka, H.; Lin, Y.. (2018)
The discovery of silicon oxide nanoparticles in space-weathered of Apollo 15 lunar soil grains
Icarus, 303, 47

Gudipati, M.S.; Castillo-Rogez, J. (2013)
The Science of Solar System Ices
Astrophysics and Space Science Library, V. 356. Springer Science + Business Media New York, 2013 ISSN 0067-0057

Halekas, J. S.; Benna, M.; Mahaffy, P. R.; Elphic, R. C.; Poppe, A. R.; Delory, G. T. (2015)
Detections of lunar exospheric ions by the LADEE neutral mass spectrometer
Geophysical Research Letters, 42, 5162

Hapke, B. (2001)
Space weathering from Mercury to the asteroid belt
Journal of Geophysical Research, 106, 10039

Harlow, G. E.; Tsujimori, T.; Sorensen, S. S. (2015)
Jadeitites and Plate Tectonics
Annual Review of Earth and Planetary Sciences, 43, 105

Helled, R.; Nettelmann, N.; Guillot, T. (2020)
Uranus and Neptune: Origin, Evolution and Internal Structure
Space Science Reviews, 216, id.38

Henning, T. (2010)
Cosmic Silicates
Annual Review of Astronomy and Astrophysics, 48, 21

Hijazi, H.; Langlinay, T.; Rothard, H.; Boduch, P.; Ropars, F.; Cassimi, A.; *et al.* (2014)
Strong perturbation effects in heavy ion induced electronic sputtering of lithium fluoride
The European Physical Journal D, 68, 6

Hilchenbach, M.; Hovestadt, D.; Klecker, B.; Möbius, E. (1993)
Observation of energetic lunar pick-up ions near Earth
Advances in Space Research, 13, 321

Hunten, D. M.; Sprague, A. L. (1997)
Origin and character of the lunar and mercurian atmospheres
Advances in Space Research,19, 1551

Ichimura, S.; Seto, Y.; Tomeoka, K. (2017)
Nepheline formation in chondrite parent bodies: Verification through experiments

Geochimica et Cosmochimica Acta, 210, 114

Iza, P.; Sigaud, R.; Farenzena, L. S.; Ponciano, C. R.; da Silveira, E. F. (2005)
Track Electrostatic Model for Describing Secondary Ion Emission of Insulators
Brazilian Journal of Physics, 35, 921

Johnson, R. E.; Baragiola, R. (1991)
Lunar surface: Sputtering and secondary ion mass spectrometry
Geophysical Research Letters, 18, 2169

Johnson, K. (2021)
Cosmology, astrobiology, and the RNA world. Just add quintessential water
International Journal of Astrobiology, 1, 4

Kiesewetter, J.; Okretic, S.; Baumann, F. M.; Brinkmann, K. -Th.; Freiesleben, H. *et al.* (1992)
Precise determination of mean velocities of fragments from spontaneous fission of ^{252}Cf
Nuclear Instruments and Methods in Physics Research Section A, 314, 125

Killen, R. M.; Bida, T. A.; Morgan, T. H. (2005)
The calcium exosphere of Mercury
Icarus, 173, 300

Killen, R.; Cremonese, G.; Lammer, H.; Orsini, S.; Potter, A. E. ; Sprague, A. L.; *et al.* (2007)
Processes that Promote and Deplete the Exosphere of Mercury
Space Science Reviews, 132, 433

Killen, R.; Cremonese, G.; Lammer, H.; Orsini, S.; Potter, A. E.; Sprague, A. L.; Wurz, P. *et al.* (2008)
Processes that Promote and Deplete the Exosphere of Mercury
Space Science Reviews, 132, 433

Leblanc, F.; Chassefière, E.; Johnson, R. E.; Hunten, D. M.; Kallio, E.; Delcourt, D. C. *et al.* (2007)
Mercury's exosphere origins and relations to its magnetosphere and surface
Planetary and Space Science, 55, 1069

Leblanc, F.; Doressoundiram, A. (2011)
Mercury exosphere. II. The sodium/potassium ratio
Icarus, 211, 10

Longobardo, A.; Della Corte, V.; Rotundi, A.; Fulle, M.; Rinaldi, G.; Formisano, M. *et al.* (2020)
67P/Churyumov-Gerasimenko's dust activity from pre- to post-perihelion as detected by Rosetta/GIADA
Monthly Notices of the Royal Astronomical Society, 496, 125

Lumpkin, G. R. (1980)
Nepheline and Sodalite in a Barred Olivine Chondrule from the Allende Meteorite
Meteoritics, 15, 139

Marchi, S.; Brunetto, R.; Magrin, S.; Lazzarin, M.; Gandolfi, D. (2005)
Space weathering of near-Earth and main belt silicate-rich asteroids: observations and ion irradiation experiments
Astronomy and Astrophysics, 443, 769-775

Macfarlane, R. D.; Torgerson, D. F. (1976)
Californium-252 Plasma Desorption Mass Spectroscopy
Science, 191, 920

Martinez, R.; Ponciano, C. R.; Farenzena, L. S.; Iza, P.; Homem, M. G. Pe; *et al.* (2006)

Ion cluster desorption from frozen NH_3 induced by impact of fast multi-charged ions
International Journal of Mass Spectrometry, 253, 1-2, 112

Martinez, R.; Ponciano, C. R.; da Silveira, E. F. (2012)
Secondary ion emission dynamics of solid ammonia bombarded by heavy ions
The European Physical Journal D, 66, 251

Martinez, R.; Bordalo, V.; da Silveira, E. F.; Boechat-Roberty, H. M. (2014)
Production of NH_4^+ and OCN^- ions by the interaction of heavy-ion cosmic rays with CO-NH_3 interstellar ice
Monthly Notices of the Royal Astronomical Society, 444, 3317-3327

Martinez, R.; Langlinay, Th.; Ponciano, C. R.; da Silveira, E. F.; Palumbo, M. E. *et al.* (2017)
Sputtering of sodium and potassium from nepheline: Secondary ion yields and velocity spectra
Nuclear Inst. and Methods in Physics Research, B, 406, 523

Martinez, R.; Agnihotri, A. N.; Boduch, Ph.; Domaracka, A.; Fulvio, D.; Muniz, G. *et al.* (2019)
Production of Hydronium Ion $(H_3O)^+$ and Protonated Water Clusters $(H_2O)_nH^+$ after Energetic Ion Bombardment of Water Ice in Astrophysical Environments
Journal of Physical Chemistry A, 123, 8001

Mennella, V.; Baratta, G. A.; Esposito, A.; Ferini, G.; Pendleton, Y. J. (2003)
The Effects of Ion Irradiation on the Evolution of the Carrier of the 3.4 Micron Interstellar Absorption Band
The Astrophysical Journal, 587, 727

Mewaldt, R. A.; Mason, G. M.; Gloeckler, G.; Christian, E. R.; Cohen, C. M. S. *et al.* (2001)
Long-Term Fluences of Energetic Particles in the Heliosphere
AIP Conference Proceedings, 598, 165

Mewaldt, R. A.; Cohen, C. M. S.; Mason, G. M.; Haggerty, D. K.; Desai, M. I. (2007)
Long-Term Fluences of Solar Energetic Particles from H to Fe
Space Science Reviews, 130, 323

Milillo, A.; Wurz, P.; Orsini, S.; Delcourt, D.; Kallio, E.; Killen, R. M.; Lammer, H. *et al.* (2005)
Surface-Exosphere-Magnetosphere System of Mercury
Space Science Reviews, 117, 397

Milillo, A.; Fujimoto, M.; Kallio, E.; Kameda, S.; Leblanc, F.; Narita, Y.; Cremonese, G. *et al.* (2010)
The BepiColombo mission: An outstanding tool for investigating the Hermean environment
Planetary and Space Science, 58, 40

Millar, T. J.; Walsh, C.; Field, T. A. (2017)
Negative Ions in Space
Chemical Reviews, 117, 1765

Nervik, W. E.. (1960)
Spontaneous Fission Yields of Cf252
Physical Review, 119, 1685

Ohtani, E.; Ozawa, S.; Miyahara, M. (2017)
Jadeite in shocked meteorites and its textural variations
Journal of Mineralogical and Petrological Sciences, 112, 247

Oliveira, P. R. B.; Martinez, R.; Fulvio, D.; da Silveira, E. F. (2021)
Energetic Ion Irradiation of N_2O Ices Relevant for Solar System Surfaces
Monthly Notices of the Royal Astronomical Society, 502, 1423

Orsini, S.; Livi, S.; Torkar, K.; Barabash, S.; Milillo, A.; Wurz, P.; di Lellis, A. M.; Kallio, E.; SERENA Team. (2010)
SERENA: A suite of four instruments (ELENA, STROFIO, PICAM and MIPA) on board BepiColombo-MPO for particle detection in the Hermean environment
Planetary and Space Science, 58, 166

Ozawa, S.; Miyahara, M.; Ohtani, E.; Koroleva, O.N.; Ito, Y.; Litasov, K.D.; Pokhilenko, N.P. (2014)
Jadeite in Chelyabinsk meteorite and the nature of an impact event on its parent body
Scientific Reports, 4, id. 5033

Paral, J.; Trávníček, P. M.; Rankin, R.; Schriver, D. (2010)
Sodium ion exosphere of Mercury during MESSENGER flybys
Geophysical Research Letters, 37, L19102

Plainaki, C.; Milillo, A.; Orsini, S.; Mura, A.; De Angelis, E.; Di Lellis, A. M.; Dotto, E. *et al.* (2009)
Space weathering on near-Earth objects investigated by neutral-particle detection
Planetary and Space Science, 57, 384

Pieters, C. M. & Noble, S. K. (2016)
Space weathering on airless bodies
Journal of Geophysical Research: Planets, 121, 1865

Ponciano, C. R.; da Silveira, E. F. (2002)
Modeling Metastable Ion Time-of-Flight Peaks
The Journal of Physical Chemistry A, 106, 10139

Ponciano, C. R.; Martinez, R.; da Silveira, E. F. (2007)
Fragmentation of $(LiF)_nLi^+$ clusters in the acceleration region of TOF spectrometers
Journal of Mass Spectrometry, 42, 1300

Poppe, A.R.; Halekas, J.S.; Sarantos, M.; Delory, G.T. (2013)
The self-sputtered contribution to the lunar exosphere
Journal of Geophysical Research: Planets, 118, 1934

Potter, A. E.; Morgan, T. H. (1986)
Potassium in the atmosphere of Mercury
Icarus, 67, 336

Potter, A. E.; Morgan, T. H. (1987)
Variation of sodium on mercury with solar radiation pressure
Icarus, 71, 472

Potter, A. E.; Morgan, T. H. (1997)
Sodium and potassium atmospheres of Mercury
Planetary and Space Science, 45, 95

Ringwood, A. E. (1976)
Limits on the Bulk Composition of the Moon
Icarus, 28, 325

Schmidt, K. -H.; Kelić, A.; Ricciardi, M. V. (2008)
Experimental evidence for the separability of compound-nucleus and fragment properties in fission
EPL (Europhysics Letters), 83, 32001

Seperuelo-Duarte E.; Domaracka, A.; Boduch, P.; Rothard, H.; Dartois, E.; da Silveira E. F. (2010)
Laboratory simulation of heavy-ion cosmic-ray interaction with condensed CO

Astronomy and Astrophysics, 512, A71

Shi, M.; Grosjean, D. E.; Schou, J.; Baragiola, R. A. (1995)
Particle emission induced by ionization tracks in water ice
Nuclear Instruments and Methods in Physics Research, B, 96, 524

Shimoda, G.; Nakamura, N.; Kimura, M.; Kani, T.; Nohda, S.; Yamamoto, K. (2005)
Evidence from the Rb-Sr system for 4.4 Ga alteration of chondrules in the Allende (CV3) parent body
Meteoritics & Planetary Science, 40,1059

Sigmund, P. (1981)
Sputtering by Ion Bombardment: Theoretical Concepts
in *Sputtering by Particle Bombardment I*, ed. by Behrish R. New York: Springer

Smyth, J.R. (1986)
Crystal Structure Refinement of a Lunar Anorthite, AN94
Journal of Geophysical Research 91, B13, E91-E97

Sprague, A. L.; Roush, T. L. (1998)
Comparison of Laboratory Emission Spectra with Mercury Telescopic Data
Icarus, 133, 174

Sprague, A.; Warell, J.; Cremonese, G.; Langevin, Y.; Helbert, J.; Wurz, P.; Veselovsky, I. (2007)
Mercury's Surface Composition and Character as Measured by Ground-Based Observations
Space Science Reviews, 132, 399

Steinbrüchel, Ch. ; Gruen, D. M. (1980)
Absolute measurement of sputtered ion fractions using matrix isolation spectroscopy
Surface Science, 93, 299

Steinbrüchel, Ch. ; Gruen, D. M. (1981)
Measurement of neutral and ion sputtering yields by matrix isolation spectroscopy
Journal of Vacuum Science and Technology, 18, 235

Stern, S. A. (1999)
The lunar atmosphere: History, status, current problems, and context
Reviews of Geophysics, 37, 453

Strazzulla, G.; Brucato, J. R.; Cimino, G.; Leto, G.; Spinella, F. (1995)
Interaction of solar wind ions with planetary surfaces
Advances in Space Research, 15, 13

Strazzulla, G.; Dotto, E.; Binzel, R.; Brunetto, R.; Barucci, M. A.; Blanco, A.; Orofino, V. (2005)
Spectral alteration of the Meteorite Epinal (H5) induced by heavy ion irradiation: a simulation of space weathering effects on near-Earth asteroids
Icarus 174, 31

Strazzulla, G. (2011)
Cosmic ion bombardment of the icy moons of Jupiter
Nuclear Instruments and Methods in Physics Research Section B, 269, 842

Szenes, G.; Kovács, V. K.; Pécz, B.; Skuratov, V. (2010)
The Effect of Heavy Cosmic-Ray Ions on Silicate Grains in the Interstellar Dust
The Astrophysical Journal, 708, 288

Szenes, G.; Kovács, V. K.; Pécz, B.; Skuratov, V. (2010)

The Effect of Heavy Cosmic-Ray Ions on Silicate Grains in the Interstellar Dust
The Astrophysical Journal, 708, 288

Takahashi, F.; Shimizu, H.; Tsunakawa, H. (2019)
Mercury's anomalous magnetic field caused by a symmetry-breaking self-regulating dynamo
Nature Communications, 10, 208

Toulemonde, M.; Assmann, W.; Ban-d'Etat, B.; Bender, M.; Bergmaier, A.; Boduch, P. *et al.* (2020)
Sputtering of LiF and other halide crystals in the electronic energy loss regime
The European Physical Journal D, 74, 144

Weber, I.; Stojic, A. N.; Morlok, A.; Reitze, M. P.; Markus, K.; Hiesinger, H. *et al.* (2020)
Space weathering by simulated micrometeorite bombardment on natural olivine and pyroxene: A coordinated IR and TEM study
Earth and Planetary Science Letters, 530, 115884

Wenk, H.R.; Joswig, W.; Tagai, T.; Korekawa, M.; Smith, B.K. (1980)
The average structure of An 62-66 labradorite
American Mineralogist 65, 81-95

Wiens, R. C.; Burnett, D. S.; Calaway, W. F.; Hansen, C. S.; Lykke, K. R.; Pellin, M. J. (1997)
Sputtering Products of Sodium Sulfate: Implications for Io's Surface and for Sodium-Bearing Molecules in the Io Torus
Icarus, 128, 386

Williams, J.S. and Poate, J.M. (1984)
Ion Implantation and Beam Processing
Academic Press Australia, 1984 ISBN 978-0-12-756980-2

Williams, R. (1965)
Photoemission of Electrons from Silicon into Silicon Dioxide
Physical Review, 140, 569

Wooden, D. H. (2008)
Cometary Refractory Grains: Interstellar and Nebular Sources
Space Science Reviews, 138, 75

Wu, W.; Xu, Y-G.; Zhang, Z-F.; Li, X. (2020)
Calcium isotopic composition of the lunar crust, mantle, and bulk silicate Moon: A preliminary study
Geochimica et Cosmochimica Acta, 270, 313

Wurz, P.; Rohner, U.; Whitby, J. A.; Kolb, C.; Lammer, H.; Dobnikar, P. *et al.* (2007)
The lunar exosphere: The sputtering contribution
Icarus, 191, 486

Wurz, P.; Whitby, J. A.; Rohner, U.; Martín-Fernández, J. A.; Lammer, H.; Kolb, C. (2010)
Self-consistent modelling of Mercury's exosphere by sputtering, micro-meteorite impact and photon-stimulated desorption
Planetary and Space Science, 58, 1599

Yokota, S.; Saito, Y.; Asamura, K.; Tanaka, T.; Nishino, M.N.; Tsunakawa, H.; Shibuya, H. (2009)
First direct detection of ions originating from the Moon by MAP-PACE IMA onboard SELENE (KAGUYA)
Geophysical Research Letters, 36, L11201

Yokota, S.; Tanaka, T.; Saito, Y.; Asamura, K.; Nishino, M.N.; Fujimoto, M.; Tsunakawa, H. (2014)

Structure of the ionized lunar sodium and potassium exosphere: Dawn-dusk asymmetry
Journal of Geophysical Research: Planets, 119, 798

Zurbuchen, T. H.; Gloeckler, G.; Raines, J.; Krimigis, S. M.; McNutt, R. L., Jr.; Solomon, S. C. (2008)
MESSENGER Observations of the Composition of Mercury's Ionized Exosphere and Heliospheric Environment
Science, 321, 90

Table 1: Absolute prompt desorption yields Y_{ion} of the most relevant ionic species desorbed from the silicate samples at room temperature after ^{252}Cf fission-fragment impacts.

SILICATE	Positive Ions			Negative Ions		
	m/q	Species	Ions impact^{-1}	m/q	Species	Ions impact^{-1}
Anorthite	1	H^+	0.2300	60	SiO_2^-	0.03278
	23	Na^+	0.0417	120	$(SiO_2)_2^-$	0.00276
	27	Al^+	0.0340	180	$(SiO_2)_3^-$	0.00156
	39	K^+	0.0654	71	$AlSiO^-$	0.00291
	40	Ca^+	0.0302	87	$AlSiO_2^-$	0.00129
				103	$AlSiO_3^-$	0.00236
				119	$AlSiO_4^-$	0.00810
Jadeite	1	H^+	0.1338	60	SiO_2^-	0.0337
	23	Na^+	0.3633	120	$(SiO_2)_2^-$	0.0034
	27	Al^+	0.0138	71	$AlSiO^-$	0.0054
	39	K^+	0.0374	87	$AlSiO_2^-$	0.0010
	50	$NaAl^+$	0.0058	103	$AlSiO_3^-$	0.0037
				119	$AlSiO_4^-$	0.0207
Nepheline	1	H^+	0.1026	60	SiO_2^-	0.0460
	23	Na^+	0.2511	120	$(SiO_2)_2^-$	0.0028
	27	Al^+	0.0037	180	$(SiO_2)_3^-$	0.0021
	39	K^+	0.1023	Σ	$(AlSi)O_n^-$	0.0750
	46	Na_2^+	0.0072			
	Σ	$Al_3O_n^+$	0.0777			

Table 2: Absolute prompt desorption yields Y_i of positive, negative and total species desorbed from the silicate samples at room temperature after ^{252}Cf fission-fragment impacts.

SILICATE	$Y_{i,pos}$	$Y_{i,neg}$	$Y_{i,total}$
Anorthite	0.56098	0.05401	**0.61449**
Jadeite	0.60177	0.06788	**0.66965**
Nepheline	0.67051	0.12585	**0.79636**

FIGURE CAPTIONS

Figure 1. Schematic representation of the PDMS-TOF-MS experimental set-up. The ion beam impinges perpendicularly from behind on the silicate film. The sputtered ions are forward ejected.

Figure 2. Electronic stopping power for each silicate: Anorthite, Jadeite, Nepheline; calculations were performed with the SRIM code. H, He, Fe and FF are considered as projectiles: Fe and FF projectile distributions are quite equivalent with a Bragg peak maximum at around $7.6x10^2$ eV/ Å, for the three silicates.

Figure 3. Mass spectrum of positive secondary ions desorbed from Anorthite, Jadeite and Nepheline, irradiated by energetic multicharged heavy ions (FF at 0.46 MeV/u) at room temperature.

Figure 4. Mass spectrum of negative secondary ions desorbed from Anorthite, Jadeite and Nepheline, irradiated by energetic multicharged heavy ions (FF at 0.46 MeV/u) at room temperature.

Figure 5. Positive Ion Yield (ions/impact) bar spectra for the three analyzed silicates and for the principal atomic and small molecular species, with mass-to-charge ratio up to 70 m/q. They have been obtained from TOF mass spectra.

Figure 6. Upper panel: Estimative of the ionic sputtering yields (Y_{ion}) after the impact of typical ^{252}Cf fission fragments on Anorthite, Jadeite and Nepheline as a function of the projectile velocity, E/m; considering the quadratic power dependence $Y_{ion} \propto S_e^2$. The inset plot shows experimental values. Lower panel: Ionic sputtering yield (Y_{ion}) simulations for nepheline showing the energy deposition dependence per unit path length (S_e), according to the power law model ($Y_{ion} \propto S_e^n$), for three values of n.

Figure 7. Sputtering rates as a function of cosmic ray energy for a typical ^{252}Cf fission fragments and Fe projectiles. Results for each projectile are very similar.

FIGURES

Fig. 1

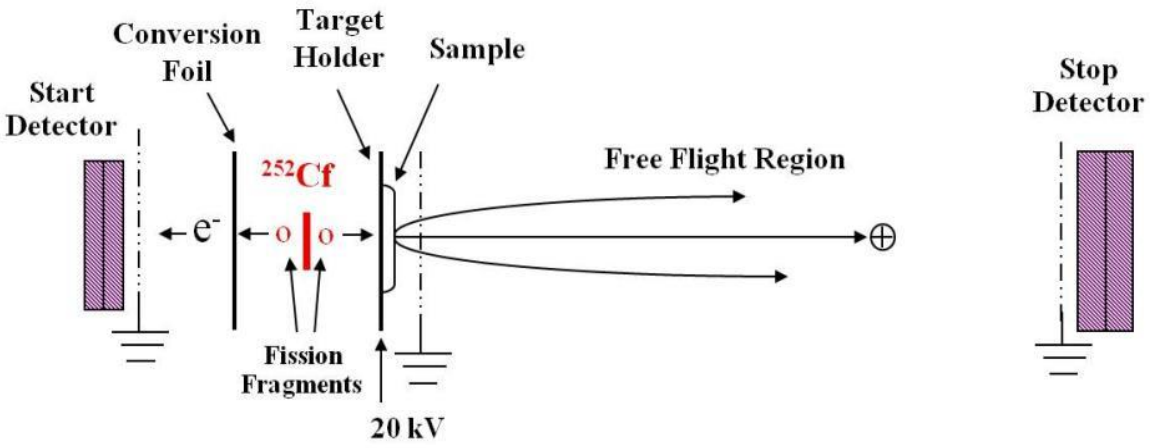

Fig. 2

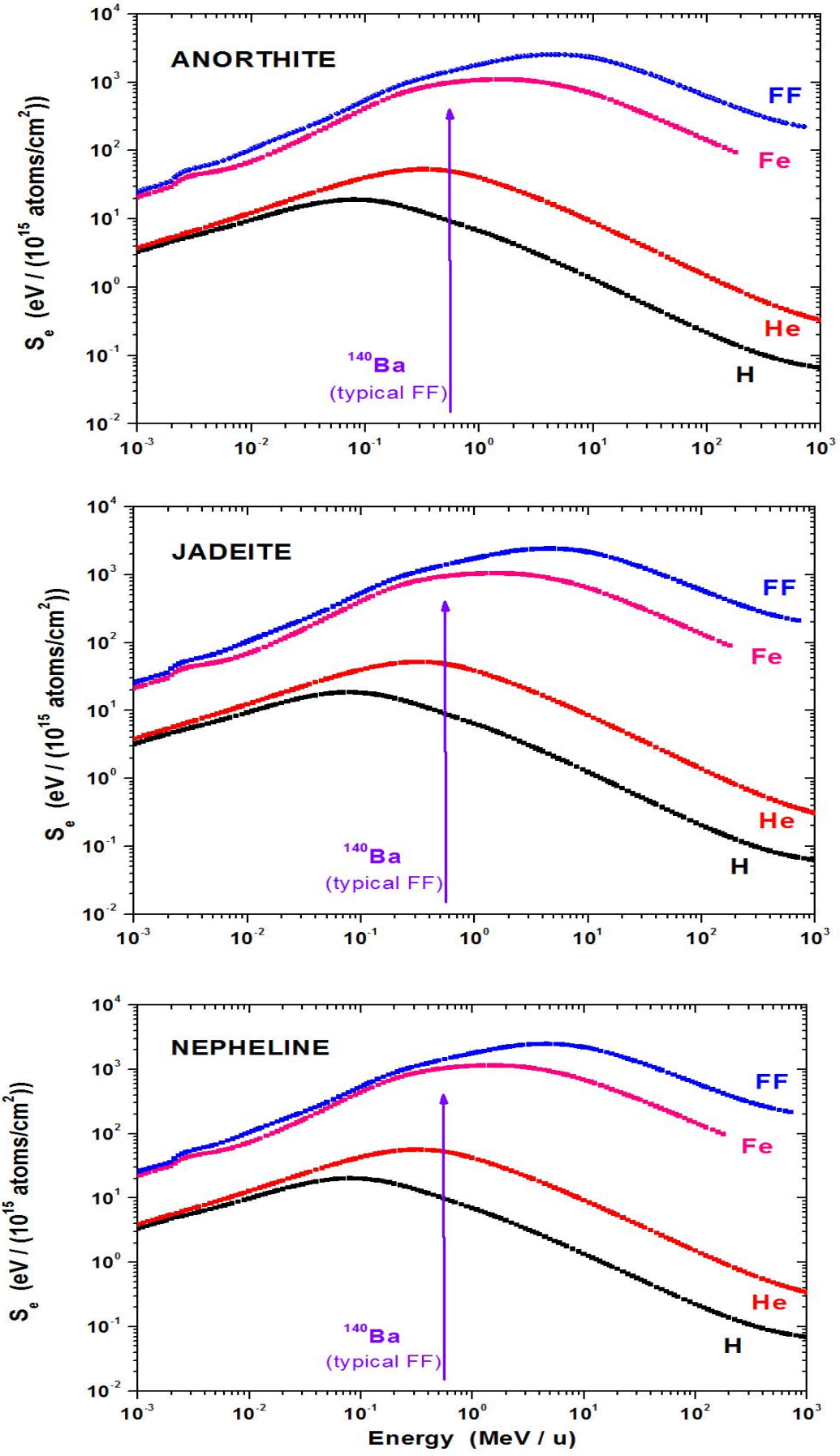
ANORTHITE
FF
Fe
He
H
^{140}Ba
(typical FF)
JADEITE
FF
Fe
He
H
^{140}Ba
(typical FF)
NEPHELINE
FF
Fe
He
H
^{140}Ba
(typical FF)
S_e (eV / (10^{15} atoms/cm^2))
Energy (MeV / u)

Fig. 3

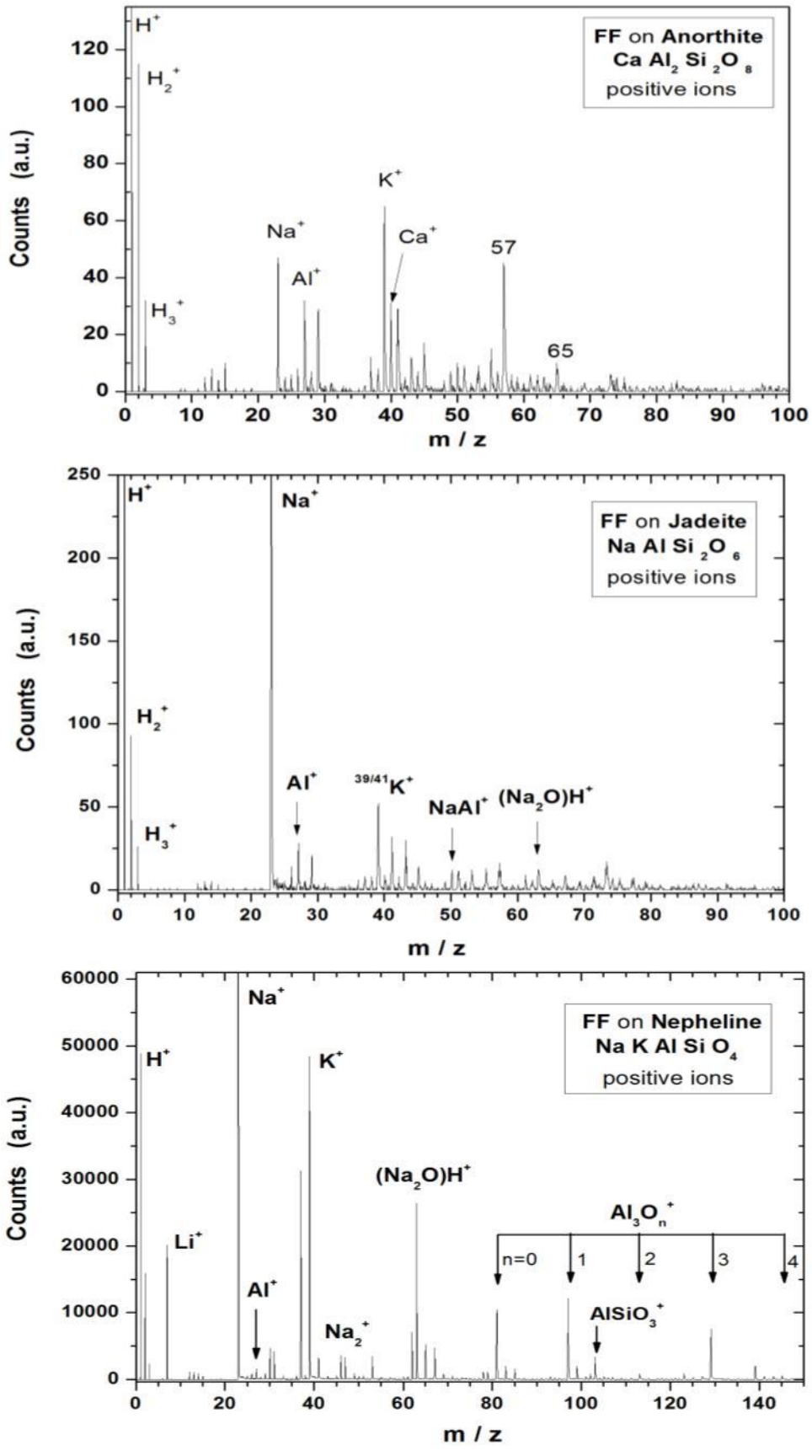
FF on Anorthite
Ca Al2 Si2 O8
positive ions
Counts (a.u.)
m / z
H+
H2+
H3+
Na+
Al+
K+
Ca+
57
65
FF on Jadeite
Na Al Si2 O6
positive ions
39/41K+
NaAl+
(Na2O)H+
FF on Nepheline
Na K Al Si O4
positive ions
Li+
Na2+
AlSiO3+
Al3On+
n=0
1
2
3
4

Fig. 4

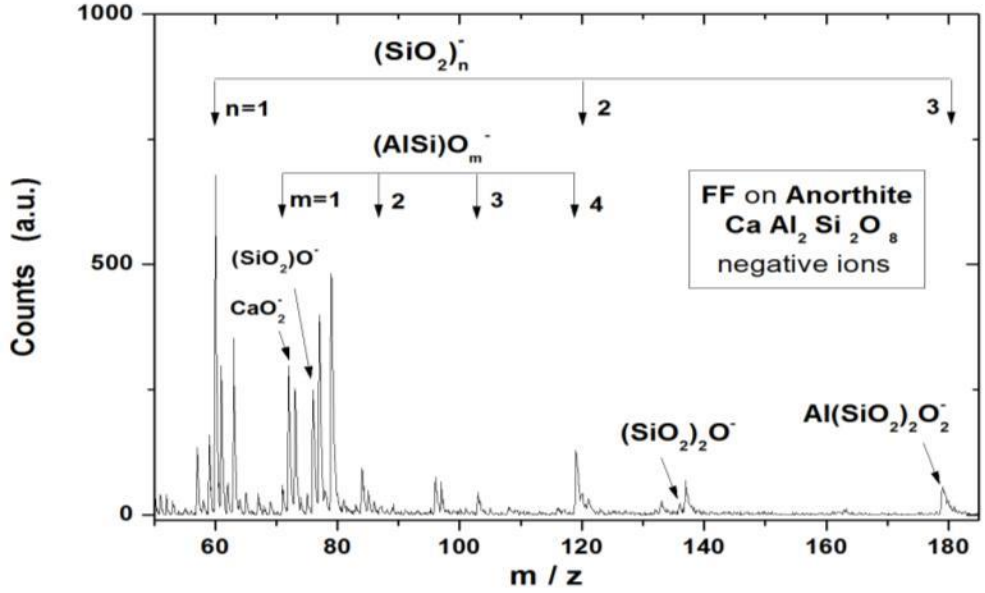
1000
500
0
Counts (a.u.)
(SiO2)n-
n=1
2
3
(AlSi)Om-
m=1
2
3
4
FF on Anorthite
Ca Al2 Si 2O 8
negative ions
(SiO2)O-
CaO2-
(SiO2)2O-
Al(SiO2)2O2-
60
80
100
120
140
160
180
m / z

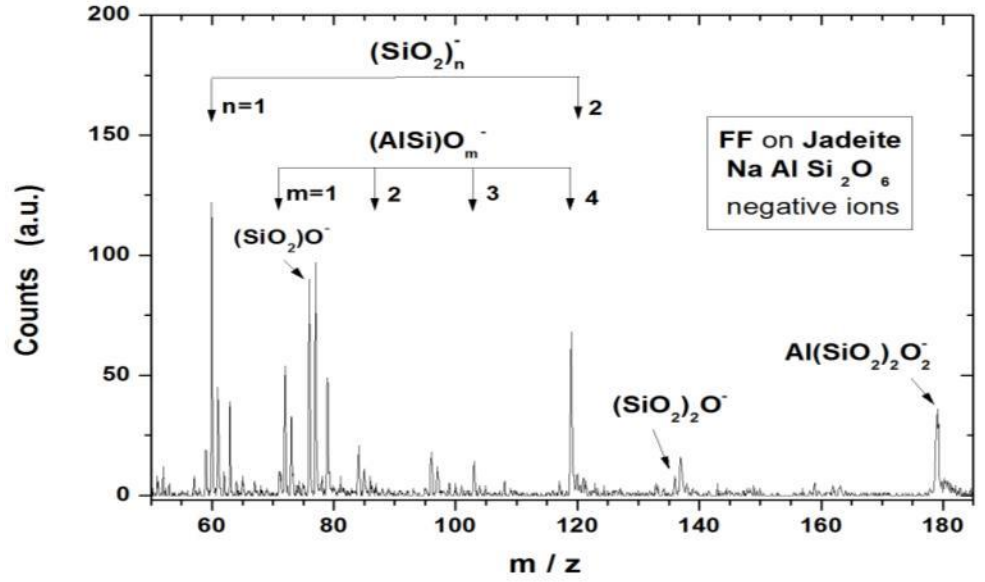
200
150
100
50
0
Counts (a.u.)
(SiO2)n-
n=1
2
(AlSi)Om-
m=1
2
3
4
FF on Jadeite
Na Al Si 2O 6
negative ions
(SiO2)O-
Al(SiO2)2O2-
(SiO2)2O-
60
80
100
120
140
160
180
m / z

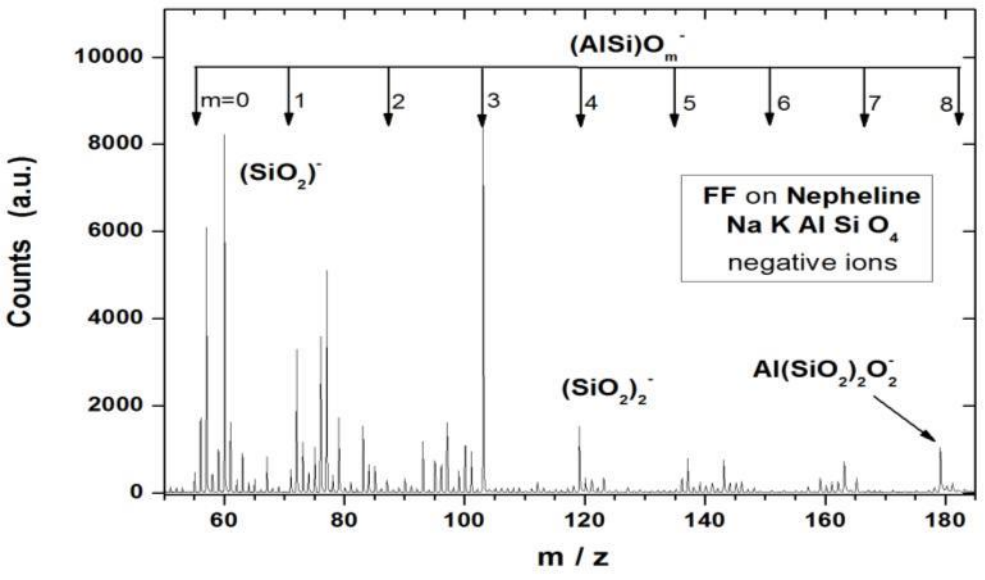
10000
8000
6000
4000
2000
0
Counts (a.u.)
(AlSi)Om-
m=0
1
2
3
4
5
6
7
8
(SiO2)-
FF on Nepheline
Na K Al Si O4
negative ions
(SiO2)2-
Al(SiO2)2O2-
60
80
100
120
140
160
180
m / z

Fig. 5

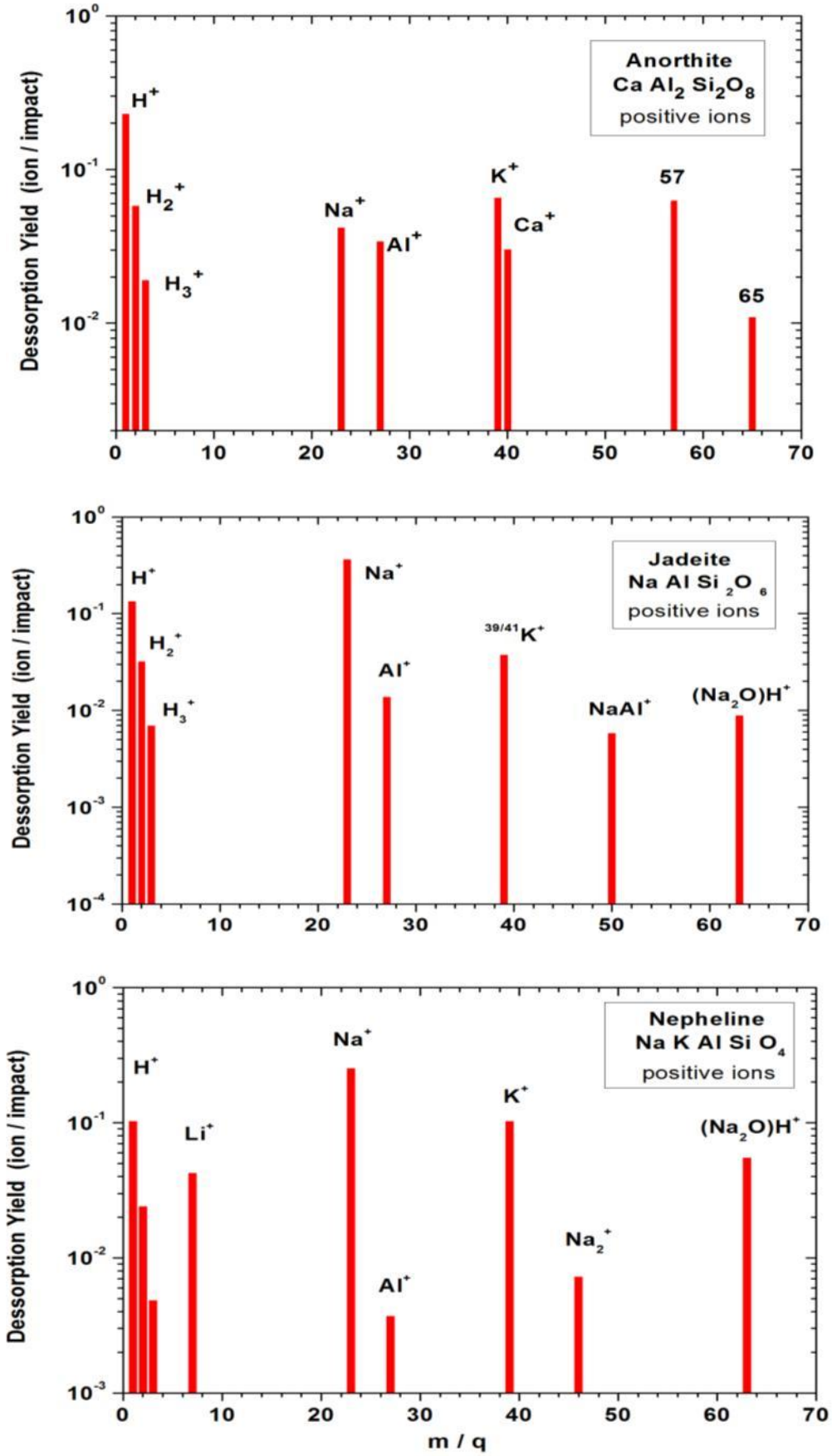
Anorthite
Ca Al2 Si2O8
positive ions
H+
H2+
H3+
Na+
Al+
K+
Ca+
57
65
Jadeite
Na Al Si 2O 6
positive ions
H+
H2+
H3+
Na+
Al+
39/41K+
NaAl+
(Na2O)H+
Nepheline
Na K Al Si O4
positive ions
H+
Li+
Na+
Al+
K+
Na2+
(Na2O)H+
Dessorption Yield (ion / impact)
m / q

Fig. 6

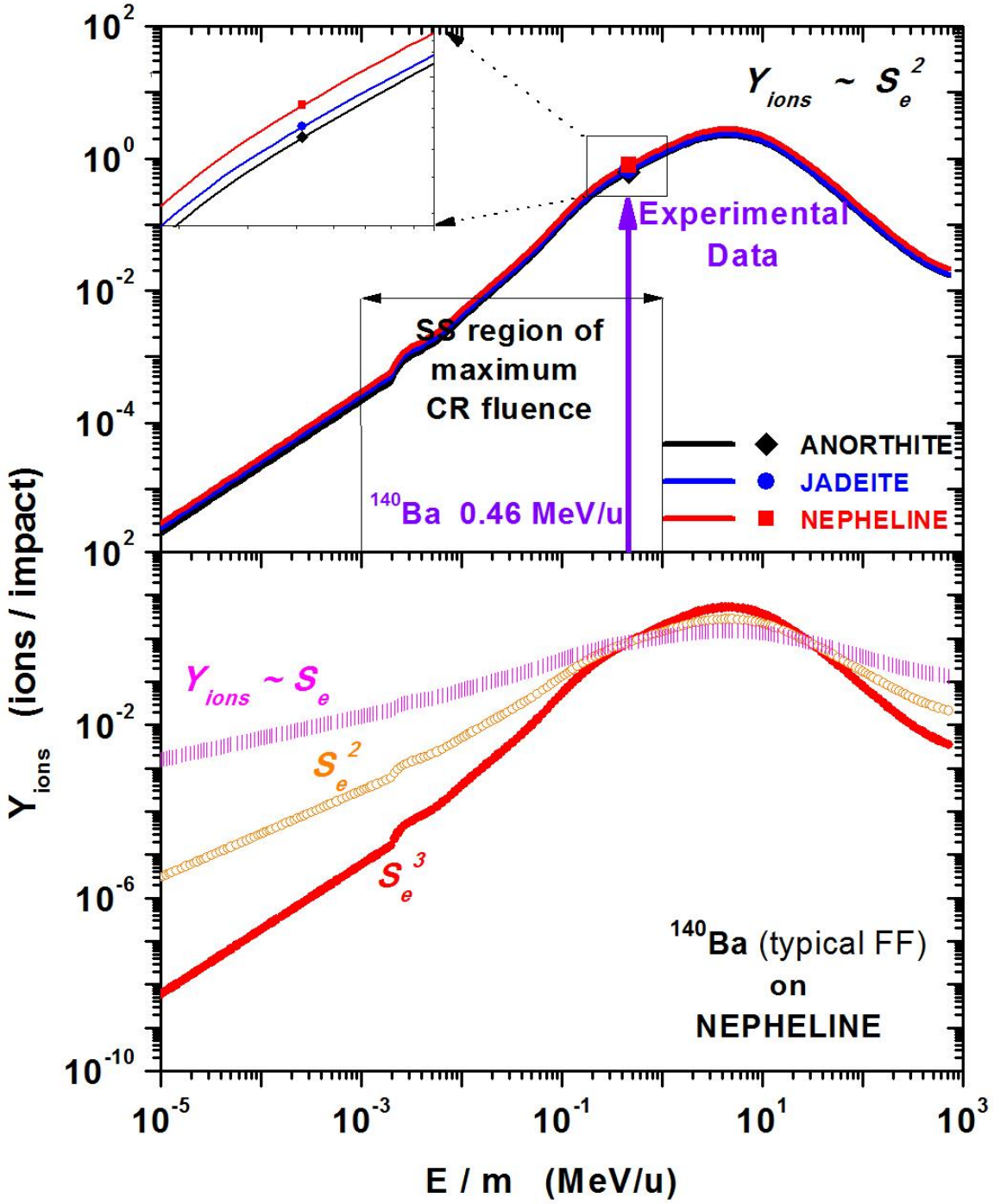
$Y_{ions} \sim S_e^2$
Experimental Data
SS region of maximum CR fluence
^{140}Ba 0.46 MeV/u
ANORTHITE
JADEITE
NEPHELINE
$Y_{ions} \sim S_e$
S_e^2
S_e^3
^{140}Ba (typical FF) on NEPHELINE
Y_{ions} (ions / impact)
E / m (MeV/u)

Fig. 7

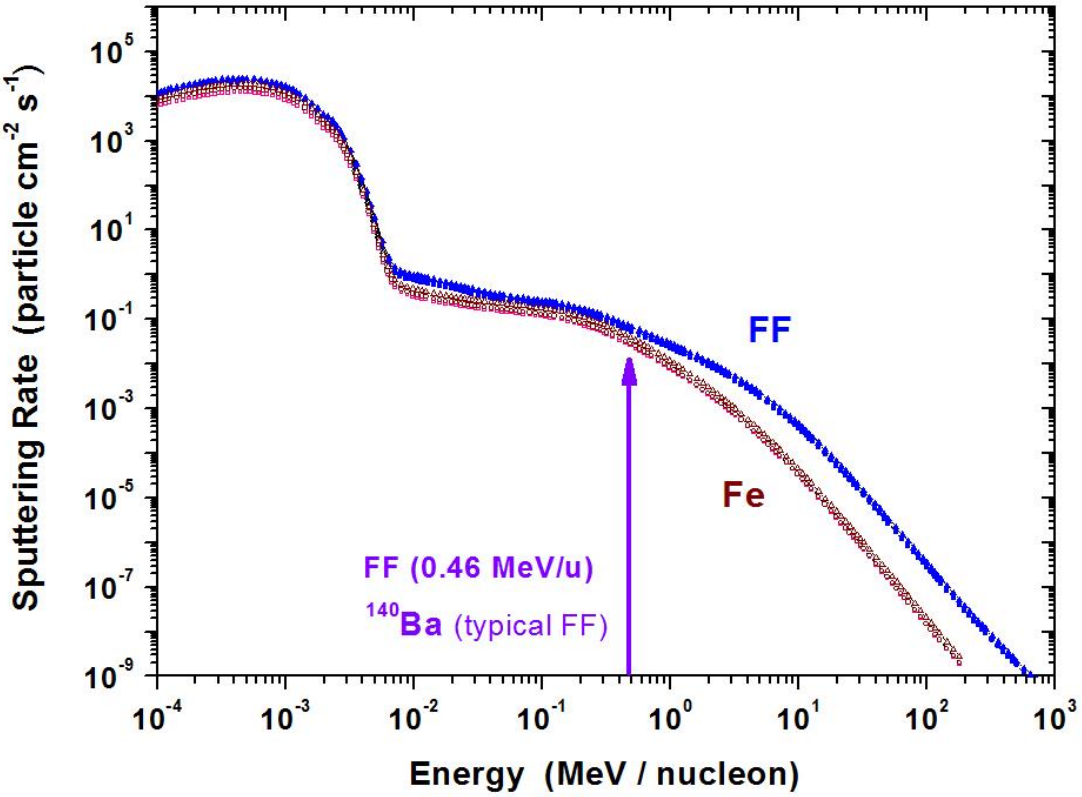
Sputtering Rate (particle cm^{-2} s^{-1})
Energy (MeV / nucleon)
FF
Fe
FF (0.46 MeV/u)
^{140}Ba (typical FF)